



HAL
open science

Statistical modeling of in-plane permeability of non-woven random fibrous reinforcement

Feifei Zhang, Sébastien Comas-Cardona, Christophe Binetruy

► **To cite this version:**

Feifei Zhang, Sébastien Comas-Cardona, Christophe Binetruy. Statistical modeling of in-plane permeability of non-woven random fibrous reinforcement. *Composites Science and Technology*, 2012, 72 (12), pp.1368 - 1379. 10.1016/j.compscitech.2012.05.008 . hal-01689206

HAL Id: hal-01689206

<https://hal.science/hal-01689206>

Submitted on 21 Jan 2018

HAL is a multi-disciplinary open access archive for the deposit and dissemination of scientific research documents, whether they are published or not. The documents may come from teaching and research institutions in France or abroad, or from public or private research centers.

L'archive ouverte pluridisciplinaire **HAL**, est destinée au dépôt et à la diffusion de documents scientifiques de niveau recherche, publiés ou non, émanant des établissements d'enseignement et de recherche français ou étrangers, des laboratoires publics ou privés.

Statistical modeling of in-plane permeability of non-woven random fibrous reinforcement

F. Zhang ^a, S. Comas-Cardona ^{a,b,*}, C. Binetruy ^{a,b}

^aEcole des Mines de Douai, Polymers and Composites Technology & Mechanical Engineering Department, 941 rue Charles Bourseul, 59508 Douai, France

^bResearch Institute in Civil Engineering and Mechanics (GeM), UMR CNRS 6183, Ecole Centrale de Nantes, University of Nantes, 1 rue de la Noe, 44321 Nantes, France

A methodology has been proposed for statistical characterization of transport behavior of a typical random fibrous medium, i.e. the Chopped Strand Mat (CSM). For any given digital images of fabric sample, statistical description of the random microstructure is employed to evaluate the permeability field, in the framework of the statistical continuum approach. By choosing suitable sampling strategy, the evaluated permeability field can be used to predict the realistic fluctuation in the flow pattern in the RTM mold-filling process with a high accuracy, as validated by the radial injection experiments. The method can be generalized to other random fibrous media. Using a database of CSM samples, statistical characterization of fiber volume fraction and permeability fields is performed respectively. Important statistical properties, e.g. the RVE size, marginal PDF and correlation length have been provided for the transport properties of the CSM, as the basis for the input data for stochastic simulation of composite processing.

Keywords: Structural composites. Transport properties. Statistics Random microstructure

1. Introduction

The Chopped Strand Mat (CSM), manufactured by stitching a random distribution of chopped strands of glass fiber into a uniform mat, is a common reinforcement of composite parts with supposed in-plane isotropic mechanical properties. Compared to traditional woven textiles, no unit periodic pattern can be observed for a random medium due to the disorderly oriented fibers forming a network of pores with arbitrary size, form and distribution. The manufacturing of composites using CSM reinforcement requires the use of resin injection techniques such as any of the Liquid Composite Molding (LCM) for instance. During such process, the resin flows within the fibrous medium. This stage is widely modeled and simulated using Darcy's law:

$$q = -\frac{K}{\mu} \nabla p \quad (1)$$

where q is the Darcy's velocity, μ is the viscosity, K is the Darcian permeability and p the fluid pressure.

Modeling such injection-based manufacturing requires a good knowledge of the permeability K . It is a fundamental property of the fibrous reinforcement whose accurate prediction is necessary for design and simulation of processing. The permeability can

either be measured experimentally or calculated using numerical simulations. On the one hand, measurements have been shown to be a tedious task which still shows high discrepancies [1]. Also the question of sample size remains opened. On the other hand, a simulation method requires to solve a Stokes (or Brinkman) flow solution using a finite element model approximating the realistic fibrous microstructure to evaluate the permeability [2,3]. In this case, the numerical domain is smaller than the experimental sample size and should be representative of the fibrous microstructure. As a result, the numerical calculation of permeability of reinforcements displaying periodic or quasi periodic structures appears easier than for random media. Therefore an appropriate technique should be used to define or estimate the microstructure of the domain in which the calculation should be performed.

Empirical formula for effective permeability of pore networks has been proposed for random porous media composed of distinctive pore and solid phases (e.g. rock) based on the statistical information obtained from digital images [4]. However, the validity of such empirical formula often depends on the length scale of the pore structure. Since the porous medium of CSM is multi-scale (e.g. 20 μm for glass fibers and few millimeters for chopped yarns) more generic homogenization techniques with statistical features could be employed.

More generally, the permeability is not spatially constant in a sample or in a preform. There is an inherent variability contained within the sample and its microstructure because of the fibrous reinforcement manufacturing or handling. This microstructural variability will lead to fluctuations in transport properties,

* Corresponding author at: Research Institute in Civil Engineering and Mechanics (GeM), UMR CNRS 6183, Ecole Centrale de Nantes, University of Nantes, 1 rue de la Noe, 44321 Nantes, France.

E-mail address: sebastien.comas@ec-nantes.fr (S. Comas-Cardona).

manufacturing and mechanical properties. A previous study focused on the propagation of the variability during the injection stage of composites manufacturing [9]. This present study is devoted to characterizing the variability of CSM (non-woven materials) which is required input for stochastic simulation tools.

The approach followed in this study will address the variability of both microstructure and permeability of CSM. The methodology is based on fibrous reinforcement digital imaging coupled with two techniques to estimate permeability from images. In Section 2, the materials and experimental procedures are detailed. Next in Section 3, the treatment of digital images, including the sampling method and statistical characterization of the random microstructure, are explained. The obtained statistical properties are employed in two different modeling approaches of effective permeability field prediction. In parallel the validation by means of the mold-filling simulation and the discussion on the effect of the representative volume element (RVE) on the results is given. Based on the validated evaluation method, the statistical properties of the permeability field are quantified in Section 4.

2. Materials and experimental procedure

The material used in this study is a CSM (M705450, Owens Corning) composed of E-glass fibers with an areal weight of 457 g/m^2 (coefficient of variation $CV = 5\%$). A total number of 37 samples of size $0.265 \text{ m} \times 0.265 \text{ m}$ are randomly selected in a roll as realizations of the random fabric.

Digital grayscale images of each sample were acquired using a lightbox device [5]. The CSM sample is placed on top of a transparent PMMA platen. White light comes from below the platen and illuminates the sample. Above the sample, a digital camera records the transmitted light as grayscale images. Local higher areal weights hinder light transmission creating dark regions, smaller areal weights do not block the light leading to brighter areas. Then image processing is performed to correct the barrel distortion and to remove any uneven lighting (Fig. 1a). Also a calibration relationship is used to related pixel intensity to the CSM areal weight [5].

Once the microstructure of each CSM sample has been recorded, the samples are then subjected to a central injection experiment.

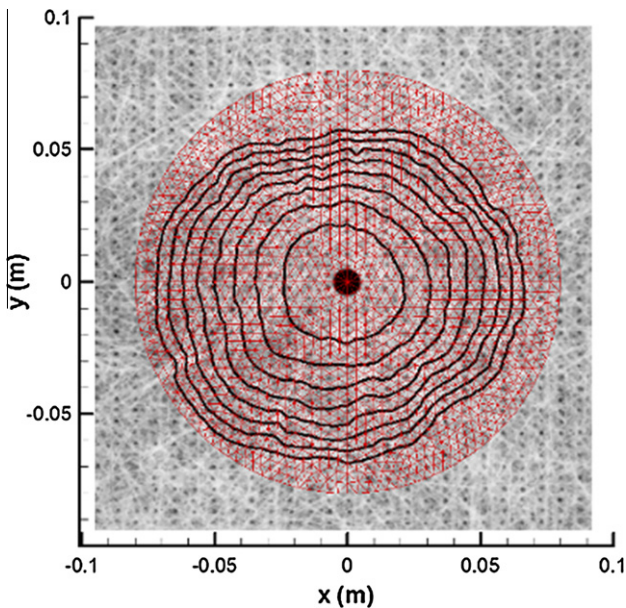


Fig. 1a. Superposition of fabric (background) and experimental flow front positions (black solid lines) detected with the CCD camera.

The injection is realized with a mineral oil whose viscosity is 0.2 Pa s . The injection pressure is kept constant at $P_{inj} = 0.05 \text{ MPa}$. The thickness of the mold cavity is adjusted to maintain an average fiber volume fraction V_f at $38\% (\pm 0.6\%)$. The bottom mold platen is made of glass and allows image recording. During the injection of each sample, several images are recorded. After appropriate image processing, the transient flow front evolution is extracted. To ease the reading of fluctuations, the flow fronts (close to circles in the Cartesian coordinates Fig. 1a) are plotted in cylindrical coordinates (θ, r) (Fig. 1b). The flow front profiles will be used in Section 3 of this article to perform validation.

3. Effective Darcian permeability evaluation

The main objective of this section is to calculate the permeability field of each sample from the images. Two routes are investigated. First, for the so-called route A, the permeability is calculated from local fiber volume fraction combined with the Kozeny–Carman model. Second, for the route B, the 1- and 2-point probability density functions (PDFs) are used with the continuum statistics. In parallel, permeability fields obtained from the two techniques are used as inputs in injection simulations and compared with experimental injections.

3.1. Kozeny–Carman model

The fiber volume fraction V_f is known to be the dominant factor for the overall flow resistance of fibrous media. The Kozeny–Carman (K–C) model of the isotropic permeability K as a function of V_f is given as:

$$K = \frac{(1 - V_f)^3}{5S_0^2 V_f^2} \quad (2)$$

where S_0 is a shape factor.

For the sake of simplicity, $N_l = 1$ in this section. In this section, the digital grayscale images obtained from the lightbox are used. In order to obtain a permeability field, a sampling strategy (Fig. 2) is defined on the original grayscale image (of size N^2 in pixels) where $N = U \times N_l \times N_A$, where $(UN_l)^2$ in pixels is the size of a sampling region S and N_A is the number of sampling regions in the image. In the end, the permeability field will be of size N_A^2 . The grayscale levels are average in each sampling region and the calibration formula given by [5] is used to calculate fiber volume fraction.

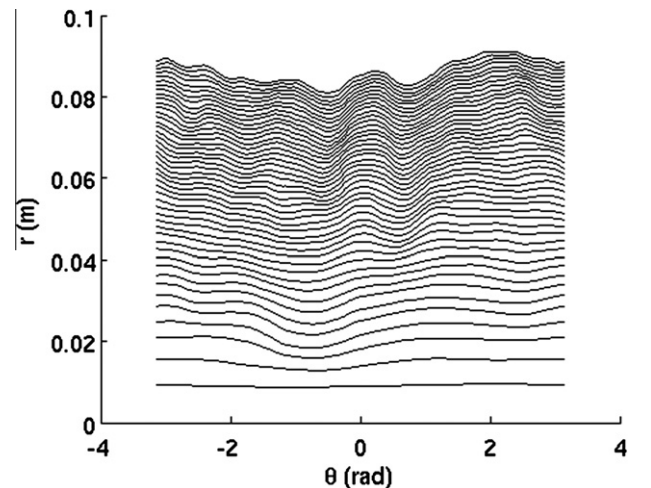


Fig. 1b. Experimental flow front positions in radial coordinates.

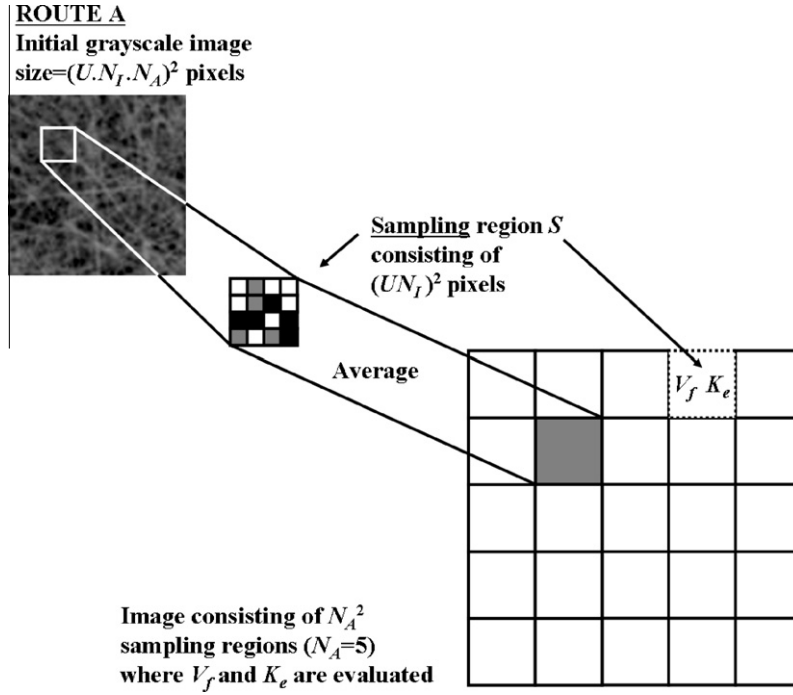


Fig. 2. Schematic of image sampling ($U = 4$, $N_f = 1$, $N_A = 5$) and procedure of route A.

As the K–C model is derived by modeling the pore structure as a bundle of ducts through which the flow is described by a generalized Poiseuille equation, the sampling region must be large enough to be a porous medium. Also considering the calibration range of the lightbox, the smallest length of a sampling region is estimated as 14 pixels (i.e. 3.2 mm) [5], resulting in a field containing 83×83 permeability values.

If the shape factor of Eq. (2) is assumed identical for close V_f , the ratio between two permeabilities K_e and K_0 can be expressed as:

$$\frac{K_e}{K_0} = \frac{(1 - V_f)^3 (V_{f0})^2}{(1 - V_{f0})^3 (V_f)^2} \quad (3)$$

The average value of K_0 at the fiber volume fraction of V_{f0} has been obtained from the injection tests performed on the 37 samples. Therefore, the permeability K_e of a region of V_f can be easily deduced using Eq. (3).

The permeability field is used as one of the input to solve Darcy's equation to simulate the experimental injection test that has been performed on each CSM sample.

To assess the effect of the permeability field, the radial injection test (at constant injection pressure) is simulated using a MATLAB code combining the FEM and the Level Set technique for modeling the moving flow front [9]. The simulated flow pattern is compared with the corresponding experimental results, in terms of the flow front radii $R(\theta_i)$ as function of direction $\theta_i \in [0, 2\pi]$ at different time instants (when the flow front is recorded in experiments). In Fig. 3a, the permeability field (normalized by the overall equivalent value) and corresponding flow pattern are displayed for the smallest sampling size of 14 pixels (3.2 mm). Although overall trend can be captured, some of the major fluctuations in the final flow front are missed by simulation. The same results are given for a larger sampling size of 20 pixels (4.6 mm) in Fig. 3b. As expected, increasing the sampling region size (i.e. smoothing spatial variability) increases the absolute error on the flow front positions (3.35% and 5.16% for 14 and 20 pixels respectively). One could argue that the sampling region size should be reduced, but the validity of Kozeny–Carman formula and Darcy's law requires region which contain enough fibers. Also, since the K–C model cannot account for

the local anisotropy due to the clustering effect, statistical continuum approach is investigated.

3.2. Statistical continuum approach

3.2.1. Image sampling

For numerical efficiency, the image is divided in single-phase units of $U \times U$ pixels (an example value $U = 3$ is used as illustration). Therefore, details on the scale less than U pixels are neglected. The pixel grayscale values are averaged within each unit. Details of the sampling and procedure are detailed in Fig. 4. Due to the nature of the statistical continuum approach, the large CSM images have to be represented as a random two-phase medium (Φ_0 and Φ_1). A threshold transformation is applied to the grayscale image to become a binary (two-phase) image (I_U) whose size is $(N_f N_A)^2$. The images have been divided into phase units and sampling regions in order to be able to check the influence of the sampling on the final results. The random microstructure in I_U is described by a phase function h :

$$h(x) = \begin{cases} 0 & x \in \Phi_0 \\ 1 & x \in \Phi_1 \end{cases} \quad (4)$$

where x denotes a unit, Φ_0 and Φ_1 denote the two phases. Since the fiber diameter (20 μm for glass) is much smaller than the scale of a unit (0.7–0.9 mm for $U = 3$), the two phases are both porous with lower V_0 (for Φ_0) or higher V_1 (for Φ_1) fiber volume fractions. As I_U is not unique, the threshold is chosen such that the two phases have equal (or very close) numbers of units.

The fiber volume fractions V_i of phases Φ_i ($i = 0, 1$) are not unique. However, if the criteria:

- the overall V_f satisfies the measured areal weight,
- V_i and the average intensity of pixels covered by phase Φ_i satisfies the calibration formula of the lightbox apparatus [5],
- V_i should not be far from the average V_f of CSM, so as that both phases are porous media,

are followed, a unique set of V_0 and V_1 can be found.

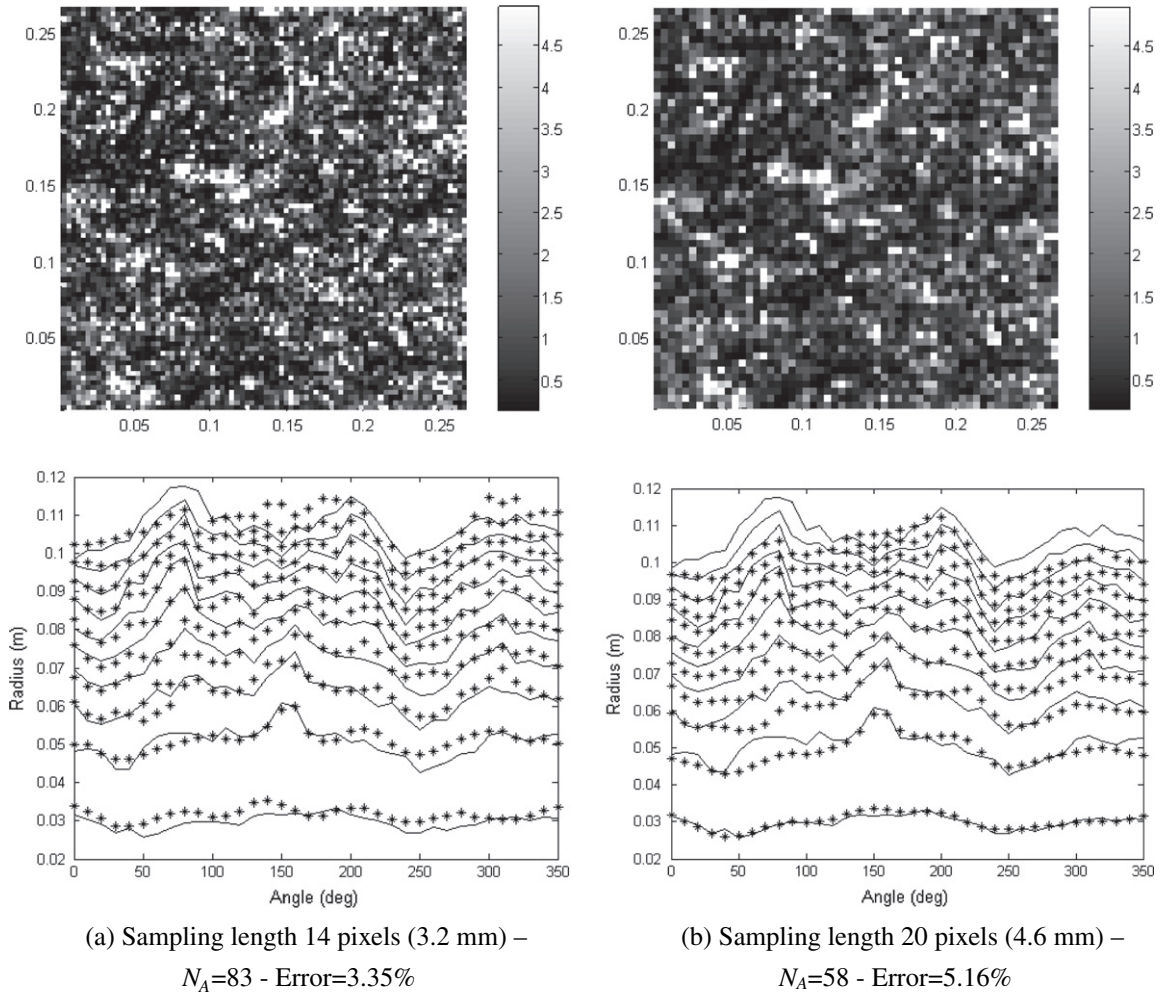


Fig. 3. Normalized permeability field (top) and flow pattern (bottom) (legend in flow pattern: line: experimental values; stars: simulated values) at normalized times: [0.0360, 0.1440, 0.2519, 0.3599, 0.4679, 0.5758, 0.6838, 0.7892, 0.8920] following route A.

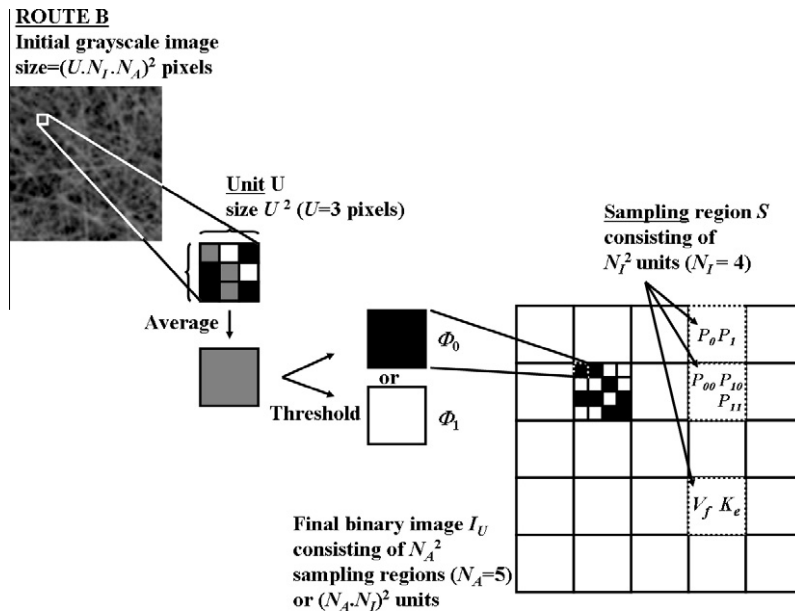


Fig. 4. Schematic of image sampling ($U = 3$, $N_f = 4$, $N_A = 5$) and procedure of route B.

3.2.2. One-point probability density function

According to [6], for a given sampling region S , the 1-point PDF P_i is the ratio between the number of units of the phase Φ_i divided by the total number of units in S . P_i represents the probability of any point occurring in the phase Φ_i . Obviously, a constraint exists as $P_0 + P_1 = 1$. Since the fiber volume fraction is a dominant factor on the permeability of a fibrous medium, it has to be calculated from the 1-point PDF. Therefore, the effective fiber volume fraction V_f in a sampling region (S) is estimated as:

$$V_f(S) = V_0 P_0 + V_1 P_1 \quad (5)$$

with V_0 and V_1 calculated as mentioned in Section 3.2.2.

3.2.3. Two-point probability density function

A heterogeneous microstructure can be completely characterized by the n -point PDFs [6] defined as the probability of n ($n = 1, 2, \dots$) points existing in a certain combination of phases. The two-point PDF is most significant for capturing the major clusters. For two points \mathbf{x} and \mathbf{x}' in the sampling regions S , the two-point PDF $P_{ij}(\mathbf{x}, \mathbf{x}')$ is defined as the probability of the vector $\mathbf{x} - \mathbf{x}'$ to be located with the head $\mathbf{x} \in \Phi_i$ and the tail $\mathbf{x}' \in \Phi_j$ ($i, j = 0, 1$).

For the sake of convenience, the one-dimensional $P_{ij}(x, x')$ defined for a certain direction θ ($0 \leq \theta < \pi$) can be used instead, which is a function of the distance $r = |\mathbf{x} - \mathbf{x}'|$ (called the lag vector). From the two-phase image, in each sampling region S , $P_{ij}(x, x')$ can be evaluated by accumulating the number of different states of (x, x') and finally normalized according to the definition of probability, i.e. $\sum_{i,j=0,1} P_{ij}(r) = 1$. For convenience, the discrete $P_{ij}(r)$ data can be fitted into appropriate analytical models, e.g. for isotropic media [7]:

$$P_{ij}(r) = P_i P_j + (-1)^{i+j} P_0 P_1 \exp(-c_{ij} r^{n_{ij}}) \quad (6)$$

where the parameters c_{ij} , n_{ij} are characteristic for a certain medium, and a correlation length can be defined as $l_{ij} = 1/c_{ij}$.

For illustration, consider a 30 mm \times 30 mm sampling region (Fig. 5a) with the corresponding two-phase image (Fig. 5b) generated by taking single-phase unit of size $U = 3$ pixels (0.7 mm). The one-point PDF in this region is calculated as $P_0 = 0.4$ and $P_1 = 0.6$. The two-point PDF $P_{ij}(r)$ is estimated in the x (Fig. 5c) and y (Fig. 5d) directions, respectively. For each of the three components ($P_{00}(r)$, $P_{11}(r)$ and $P_{01}(r) = P_{10}(r)$), data are fitted into the analytical models in Eq. (6) ($n_{ij} = 1$). The convergent values $P_{ij}(\infty) = P_i P_j$ derived from Eq. (6) are confirmed by Fig. 5c and d ($P_{00}(r) = 0.16$, $P_{11}(r) = 0.36$ and $P_{01}(r) = 0.24$). Besides, the correlation length defined above (taking as the average value $(1/c_{00} + 1/c_{01} + 1/c_{11})/3$) is estimated to be $l_x = 0.85$ mm and $l_y = 0.7$ mm (x, y denote the horizontal and vertical directions, respectively). When more samples are analyzed, the mean correlation length is found to be about 1.03 mm in the x direction and 0.86 mm in the y direction, which indicates a slight anisotropy for the microstructure (at least for the length scale less than 30 mm). The correlation lengths calculated here cannot be related to the CSM microstructure because they are directly linked to the value of U (which is a parameter chosen by the user).

So far, the tools to describe the microstructure (1- and 2-point probability density functions) have been described. In the following, the focus will be on the permeability evaluation from the microstructural characterization.

3.2.4. Statistical continuum approach

The statistical continuum approach, developed based on works of Kroner [10], Adams et al. [11], Garmestani et al. [6,8], among others, has application in predicting macroscopic behavior of heterogeneous materials and microstructure sensitive design. As the

current problem requires a permeability field containing distinctive spatial variations from region to region, each sampling region S is subjected to the statistical continuum approach to obtain the formulation of effective permeability (K_e). Therefore, the formulation of K_e is described first, followed by the analysis of the suitable sampling region size.

The effective permeability in a region is commonly evaluated by imposing a macroscopic pressure gradient ∇p_0 on the region and solving for the resulted localized pressure gradient field $\nabla p(\mathbf{x})$. For any point in the region, Darcy's law is written as:

$$q(\mathbf{x}) = -\mathbf{k}(\mathbf{x}) \cdot \nabla p(\mathbf{x}) \quad (7)$$

where the constant viscosity is included in the term $k = K/\mu$ for simplifications of the equations. According to the two-phase definition, the local permeability

$$\mathbf{k}(\mathbf{x}) = \begin{cases} k_0 & \mathbf{x} \in \Phi_0 \\ k_1 & \mathbf{x} \in \Phi_1 \end{cases} \quad (8)$$

is known as the phase permeability. Assuming the anisotropy is only induced by the clustering effect and each phase is an isotropic medium, k_i can be estimated by the K-C model using V_i (i.e. fiber volume fraction of phase Φ_i).

The heterogeneous field $\mathbf{k}(\mathbf{x})$ is equivalent to a local fluctuation field $\hat{\mathbf{k}}(\mathbf{x})$ superposed on a reference homogeneous value \mathbf{k}_m :

$$\mathbf{k}(\mathbf{x}) = k_m + \hat{\mathbf{k}}(\mathbf{x}) \quad (9)$$

with the reference value taken as the volume-average of phases:

$$k_m = k_0 P_0 + k_1 P_1 \quad (10)$$

Since $\hat{\mathbf{k}}(\mathbf{x})$ is also a two-state function with values $\hat{\mathbf{k}}(\mathbf{x}) = \mathbf{k}(\mathbf{x}) - k_m$, its spatial distribution follows the same statistical features as the microstructure.

Based on the above definition, the expectation of the statistical formulation of local pressure gradient can be derived based on the framework of the statistical continuum approach (the details are given in Appendix A in analogy to [8]):

$$\langle \nabla p(\mathbf{x}) \rangle = \nabla p_0 + \left[\int \mathbf{G}(\mathbf{x}, \mathbf{x}') * \langle \hat{\mathbf{k}}(\mathbf{x}) \rangle d\mathbf{x}' \right] \nabla p_0 \quad (11)$$

where $\langle \cdot \rangle$ denotes the expectation estimated at \mathbf{x} , $\mathbf{G}(\mathbf{x}, \mathbf{x}')$ is the Green operator (see Appendix A), and $\langle \hat{\mathbf{k}}(\mathbf{x}) \rangle$ is referred to as the two-point correlation function of $\mathbf{k}(\mathbf{x})$, evaluated as:

$$\langle \hat{\mathbf{k}}(\mathbf{x}') \rangle = f_{ij}(\mathbf{x}' \in \Phi_j | \mathbf{x} \in \Phi_i) \hat{\mathbf{k}}(\mathbf{x}') \quad (12)$$

where $f_{ij}(\mathbf{x}' \in \Phi_j | \mathbf{x} \in \Phi_i)$ is the conditional two-point PDF, defined as:

$$f_{ij}(\mathbf{x}' \in \Phi_j | \mathbf{x} \in \Phi_i) = \frac{P_{ij}(\mathbf{x}, \mathbf{x}')}{P_i} \quad (13)$$

Based on the current two-phase definition of the image, the convolution integral in Eq. (11), accounting for the dependence of local pressure gradient at \mathbf{x} on all the surrounding points $\mathbf{x}' \in S$ ($\mathbf{x}' \neq \mathbf{x}$), is evaluated by the integration (reduced to summation as the smallest unit has a single phase) over all the points except \mathbf{x} :

$$\int \mathbf{G}(\mathbf{x}, \mathbf{x}') * \langle \hat{\mathbf{k}}(\mathbf{x}) \rangle d\mathbf{x}' = \sum_{\mathbf{x}' \in S, \mathbf{x}' \neq \mathbf{x}} \left\{ \mathbf{G}_{ij}(\mathbf{x}, \mathbf{x}') \langle \hat{k}_{ij}(\mathbf{x}') \rangle \right\} \quad (14)$$

where the subscript ij denotes the component of second-order tensor. Substituting Eqs. (12)–(14) into Eq. (11), the expectation of local pressure gradient is evaluated as:

$$\langle \nabla p(\mathbf{x}) \rangle = \nabla p_0 + \sum_{\mathbf{x}' \in S, \mathbf{x}' \neq \mathbf{x}} \left\{ \mathbf{G}_{ij}(\mathbf{x}, \mathbf{x}') \frac{P_{ij}(\mathbf{x}, \mathbf{x}')}{P_i} \hat{k}_{ij}(\mathbf{x}') \right\} \quad (15)$$

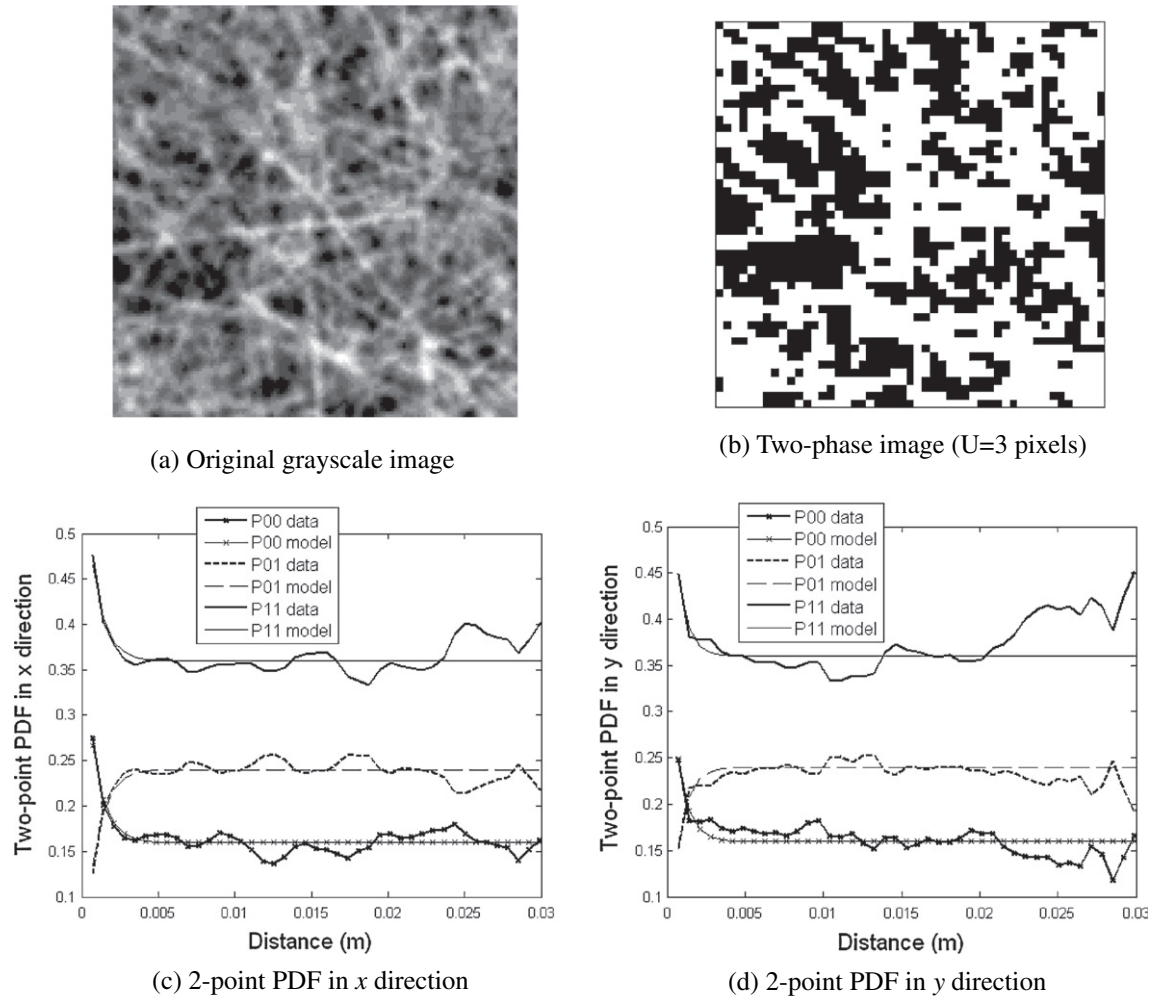


Fig. 5. Two-point PDF (for single-phase unit: 0: black, 1: white. For 2-point PDF: thick lines: experimental data; thin lines: fitted analytical model, with the same line type).

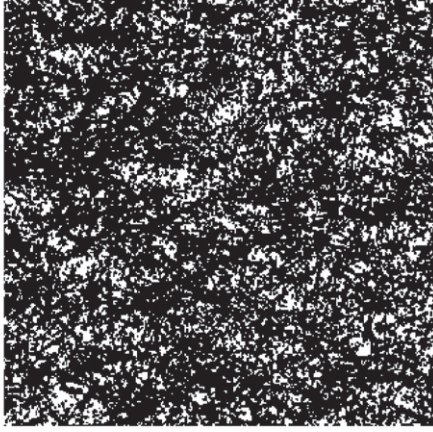
For each principal direction (e.g. x or y) of permeability, Eq. (15) is evaluated using the one and two-point PDF in the corresponding direction, and then substituted into Eq. (7) to get the expectation of local flux $\langle q(\mathbf{x}) \rangle$. After the loop over all the single-phase units in the sampling region, the averaged flux $\langle q(\mathbf{x}) \rangle$ can be obtained, from which the effective permeability (k_e) can be obtained according to:

$$\langle q(\mathbf{x}) \rangle = -k_e \nabla p_0 \quad (16)$$

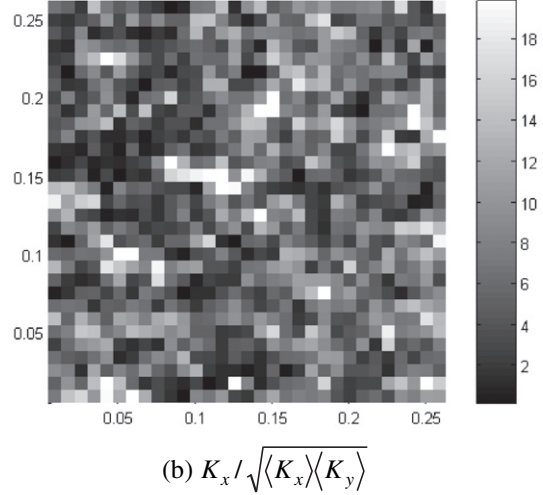
Using the above formulation, the permeability field of the same material sample as in Section 3.1 is evaluated and used to simulate the radial injection process. First, the sampling parameters are chosen to be $U = 3$ pixels (0.7 mm), the two-phase image in Fig. 6a and $N_l = 12$, resulting in sampling regions of size $9 \text{ mm} \times 9 \text{ mm}$. The permeability field K_x normalized by the value ($\sqrt{\langle K_x \rangle \langle K_y \rangle}$) and the distribution of anisotropic ratio (K_x/K_y) are displayed in Fig. 6b and c, respectively. Comparing to the K-C results in Fig. 3, much stronger fluctuation in local permeability magnitude and significant local anisotropy can be noticed in Fig. 6b and c. This effect is interesting because even though the sampling region size is larger in Fig. 6b (compared to Fig. 3a or b), it does not smooth the permeability out. Quite inversely, the local fluctuations are increased (Fig. 6b). Comparing the simulated flow pattern (stars) to the experimental results (lines), Fig. 6d shows that the fluctuation along different directions can be accurately reproduced by the numerical simulation (error or 2.32%), which means the predicted

permeability field has variations close to that of the realistic material. Therefore the cluster-induced local anisotropy and strong fluctuation are well described by the statistical continuum approach.

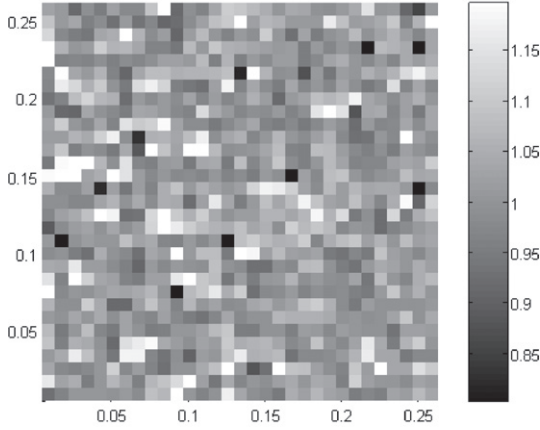
Since the microstructural statistics and permeability are evaluated for each sampling region S by integrating over all single-phase units, the resolution of the two-phase image (U) and size of sampling region control the computational effort. For a fibrous preform of large dimensions, the suitable sampling size should be a compromise between efficiency and accuracy. In order to estimate the influence of an increase in U on the precision of the response, two sampling cases with $U = 5$ or 7 pixels, respectively, are applied on the same sample. From the corresponding permeability fields (Fig. 7), the magnitude of fluctuation and anisotropy both decreases as U increases, according to the resulted flow pattern. When the original image is resampled at a resolution of $U = 5$ pixels (1.16 mm), the magnitude of the predicted fluctuation decreases, but the trend can be correctly captured (error of 2.22%). By further increasing U to 7 pixels (1.62 mm), the flow pattern is too smooth to reproduce the minor fluctuation appeared in experiments (error 3.34%), but is still acceptable if the objective is to predict the discrepancy between different directions of flow front. Besides, the parameter N_l represents the range of influence of surrounding media on any local permeability value, and dictates the computational effort. By trial of various cases, $N_l = 12-20$ (i.e. sampling region of size of 8.5–14 mm) should be a suitable choice in that the valid two-point statistics in the sampling region can be evaluated with relatively low computational cost.



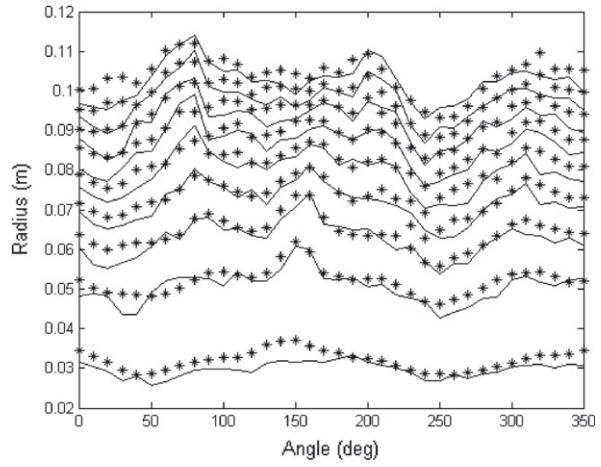
(a) Two-phase microstructure



(b) $K_x / \sqrt{\langle K_x \rangle \langle K_y \rangle}$



(c) Anisotropic ratio K_x/K_y



(d) Flow pattern at normalized times [0.0388, 0.1551, 0.2715, 0.3878, 0.5042, 0.6205, 0.7368, 0.8504, 0.9612] – Error=2.32%

Fig. 6. Permeability field and simulated flow pattern following route B ($U = 3$, $N_t = 12$, $N_A = 30$) – sampling size length 9 mm.

4. Statistical analysis of fibrous properties

4.1. Representative volume element (RVE)

Comprehensive reviews of the possible definitions of the RVE for heterogeneous media can be found, e.g. [12–14]. In some studies, the RVE size has been taken as the characteristic dimension (for effective properties) of the microstructure which can be estimated from results (e.g. the power spectral density function) of digital image analysis [3]. More generally, the RVE size is considered as function of many parameters, e.g. sample size, allowable error, the property of interest, etc. A generic definition of RVE size proposed by Kanit et al. [13] is employed here.

Consider a random function $Z(x)$ as a mapping of a phase property. The instances of $Z(x)$ include the fiber volume fraction field, $V_f(x) = V_i$ and the permeability field $K(x) = \mathbf{k}(x)/\mu$ when $x \in \Phi_i$.

Based on the framework of [13], the length of RVE (L^{RVE}) for a given relative error ε (i.e. ratio of the absolute error to the mean value \bar{Z}) and number of realizations (N) can be derived as [14]:

$$L^{RVE} = \frac{4D_Z^2 A_n}{\varepsilon^2 \bar{Z}^2 N} \quad (17)$$

The point variance of the random process $Z(x)$ is defined as [13]:

$$D_Z^2 = P_0 P_1 (Z_0 - Z_1)^2 \quad (18)$$

where P_i and Z_i denote the one-point PDF and the phase property (V_i or $\mathbf{k}(h_i)$).

Besides, an integral range (A_n) is defined for $Z(x)$ as follows [13]:

$$A_n = \frac{1}{C(Z, 0) - C(Z, 0)^2} \int_{R^n} (C(Z, r) - C(Z, 0)^2) dr \quad (19)$$

where n denotes the dimension of space, $C(Z, r)$ is the covariance function with the same meaning as the two-point PDF $P_{00}(r)$ or $P_{11}(r)$ (depending on the phase in consideration) with r as the lag distance.

Firstly, A_n and D_Z^2 are evaluated for the N samples and averaged. Both $P_{ij}(r)$ and A_n are estimated in the x and y directions, respectively. By varying the sampling size and observing the evolution, the parameters are estimated as $A_n = 1.32$ mm (in x direction), $A_n = 1.04$ mm (in y direction), $D_Z^2(V(x)) = 0.0205$, $D_Z^2(K_x(x)) = 8.251 \times 10^{-19}$ m² and $D_Z^2(K_y(x)) = 5.776 \times 10^{-19}$ m². L^{RVE} in each direction is then estimated from Eq. (17) as a function of the relative error. As shown in Fig. 8, to obtain a relative error below 5%, the RVE size for V_f should be larger than 10 mm \times 10 mm, whereas that for K_x (or K_y) has to be larger than 475 mm \times 375 mm. The much larger RVE size of the latter should be due to its dependence

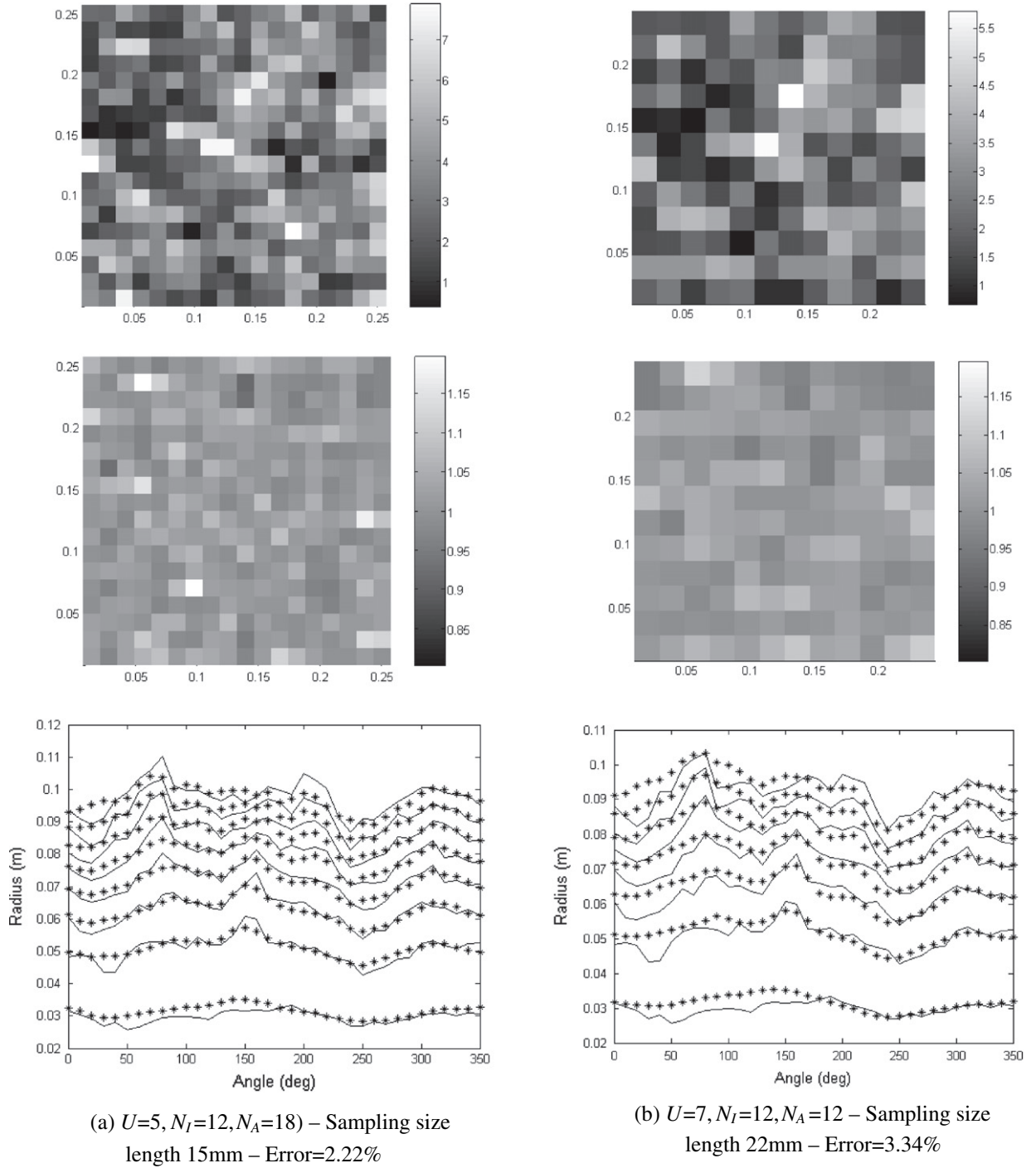


Fig. 7. Influence of single-phase unit size. (top: $K_x / \sqrt{\langle K_x \rangle \langle K_y \rangle}$; middle: anisotropic ratio K_x / K_y ; bottom: flow pattern (line: experimental values; stars: simulated values) at normalized times [0.05, 0.20, 0.35, 0.50, 0.65, 0.80, 0.95]).

on the two-point statistics of microstructure. As the typical pore size (estimated as the square root of the permeability which is taken as $3 \times 10^{-10} \text{ m}^2$) is on the scale of 10^{-2} mm , the RVE size is 3–4 magnitudes higher in length scale.

According to the physical meaning of RVE, the relationship in Fig. 8 is expected to be approximately valid for the effective property. In parallel, for various RVE sizes, the effective properties are used to get the relative error between N samples, as displayed in discrete marks in Fig. 8. Results show that, for either the fiber volume fraction or the permeability, the RVE estimated by Eq. (17) and that estimated based on the effective property have acceptable

correspondence. However, due to the expectation operation in the statistical continuum method (Eq. (11)), the relative error for the effective permeability field is slightly lower than the value given by Eq. (17), for given RVE sizes (Fig. 8b).

4.2. Marginal PDF

A reliable knowledge of the probabilistic distribution of material properties is necessary for generating the random inputs for stochastic simulation. By comparison, the marginal PDF is similar

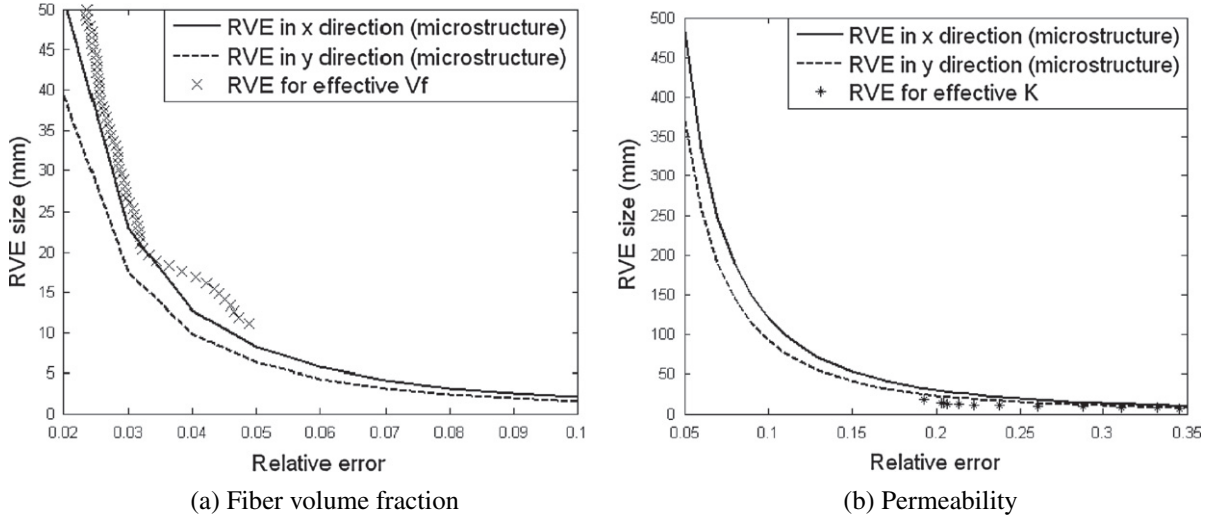


Fig. 8. RVE size with respect to various properties (curves: estimation using Eq. (17); marks: estimation using effective property).

at different locations in the field, which allows the field-averaged values of samples to be used in the further analysis.

The Maximum Entropy Principle (MEP) is a standard technique for evaluating the accurate marginal PDF from given moments of samples, without need of any assumption on the probabilistic model. The permeability component is chosen for demonstration. Due to the small magnitude (10^{-10} m^2), the logarithmic value $Y(\omega) = \log(K(\omega))$ (K in m^2) is the random variable to analyze, with the PDF denoted by $f_Y(y)$. The MEP is based on the theory that the realistic PDF ($f_Y(y)$) is the one that maximizes the information entropy H :

$$H = - \int_D f_Y(y) \log(f_Y(y)) dy \quad (20)$$

subjected to the constraints of moments of different orders:

$$\mu_i = E[Y^i] = \int_D y^i f_Y(y) dy \quad (i = 0, 1, \dots, m) \quad (21)$$

By means of the Lagrange method, the solution of the optimization problem defined by Eqs. (20) and (21) is expressed in the exponential form

$$f_Y(y) = \exp \left(-\lambda_0 - \sum_{i=1}^m \lambda_i y^i \right) \quad (22)$$

with $(m+1)$ Lagrange multipliers λ_i ($i = 0-m$) to solve for. For example, the solution based on the moments of up to the 3rd order is expressed as:

$$f_Y(y) = \exp(-\lambda_0 - \lambda_1 y - \lambda_2 y^2 - \lambda_3 y^3) \quad (23)$$

Substituting Eq. (23) into Eq. (20), a nonlinear system of equations of the unknown multipliers are obtained as

$$\mathbf{H}(\lambda) = \boldsymbol{\mu} \quad (24)$$

which can be solved using the Newton iterative method, i.e.:

$$\lambda^{i+1} = \lambda^i + [\nabla_{\lambda} \mathbf{H}(\lambda^i)]^{-1} [\boldsymbol{\mu} - \mathbf{H}(\lambda^i)] \quad (25)$$

with the 4×4 Jacobian matrix $\nabla_{\lambda} \mathbf{H}(\lambda)$ evaluated by numerical integration. Using the solved multipliers, the accurate PDF of $\log K_x$ and $\log K_y$ (K in m^2) are represented as

$$f_Y(y) = \begin{cases} \exp(-2129.3 - 620.01y - 59.797y^2 - 1.9082y^3) & (Y = \log K_x) \\ \exp(-1750.8 - 501.03y - 47.419y^2 - 1.4821y^3) & (Y = \log K_y) \end{cases} \quad (26)$$

The MEP solution of the PDF can be validated by the empirical PDF, which can be directly estimated using common statistical software (e.g. Statistical Toolbox of MATLAB) based on the non-parametric models without any assumptions on the data-producing mechanism. Besides, a chosen parametric PDF model with the parameters calculated from the moments of the raw data can also be compared to estimate the validity of the model. Various PDF results are given for V_f and K_x in Fig. 9a and b, respectively. It can be seen that both V_f and $\log(K_x)$ ($\log(K_y)$ in analogy) have a Gaussian PDF, which means that the log-normal PDF is an appropriate model for the permeability component.

4.3. Correlation length

Since the marginal PDF is approximately invariant in the random field $K(x)$, the stationary assumption is acceptable, i.e. the mean (μ_K), variance (σ_K^2) and the autocorrelation function are spatially independent. Therefore, a unique spatial correlation length can be defined for the whole random field (in each direction).

The autocorrelation function, which describes the correlation between the variations of property at any two locations with a distance r , is defined as:

$$R_K(r) = \frac{\langle [K(x) - \mu_K][K(x+r) - \mu_K] \rangle}{\sigma_K^2} \quad (27)$$

Here a 1-D form is used, which can be evaluated in different directions to describe the spatial anisotropy. Using the definition, the autocorrelation of K_x field in the x and y directions are displayed for 10 samples in Fig. 10a, showing a decaying tendency with the distance before reaching a plateau. Similar graphs can be obtained for autocorrelation of K_x in the y direction. According to the trend of data, an exponential model:

$$R_K(r) = \exp \left[-\left(\frac{r}{l}\right)^n \right] \quad (28)$$

can be fitted, where the power n is close to 1 and the parameter l , i.e. the correlation length (in the given direction), can be estimated using a nonlinear regression approach. Using an individual sample for instance, the fitted analytical model is compared to the raw data in Fig. 10b.

Due to the scatter in microstructure, the estimated correlation length has significant discrepancy between samples, especially for the permeability, as displayed in Fig. 11a-c. Since the

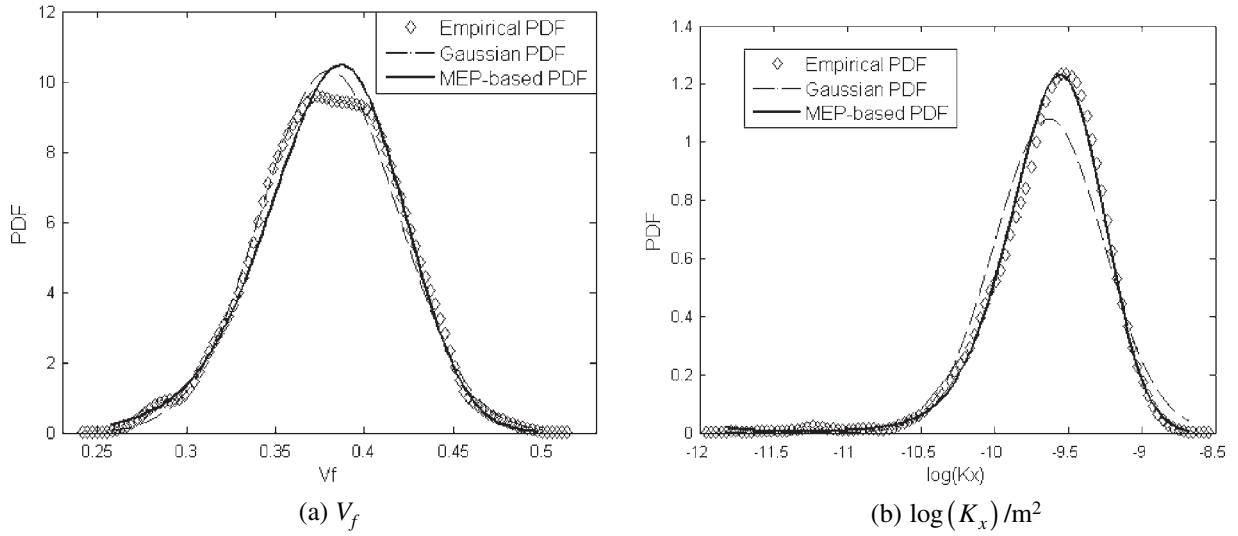


Fig. 9. Marginal PDF of fiber volume fraction and permeability.

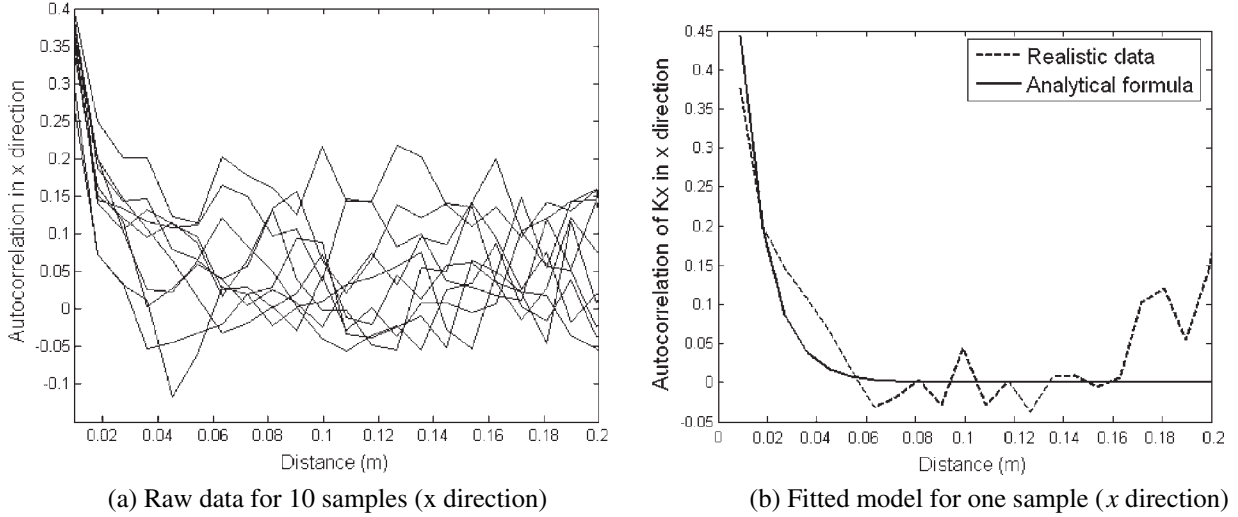


Fig. 10. Autocorrelation of permeability field K_x .

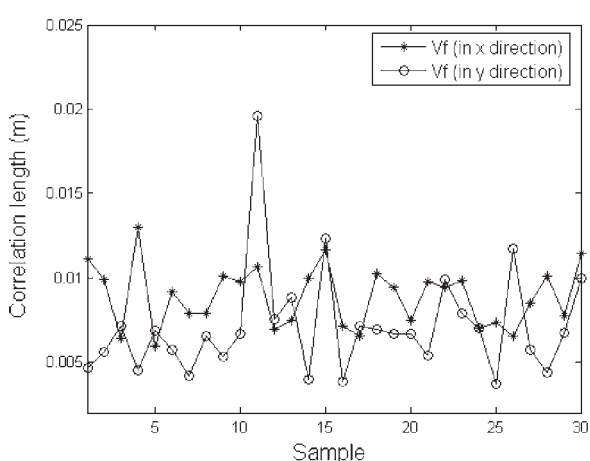
correlation length is a characteristic dimension of the microstructure, there might be a link between this dimension and the transport behavior of material. The four samples with the minimum and maximum correlation lengths are focused on. By post-processing of the flow fronts, the standard deviation (σ_R) between the flow front radii in different directions is a function of time, which is expected to increase if the flow front becomes more and more distorted when moving forward. As shown in Fig. 11d, the samples with longer correlation length has a relatively steady level of σ_R as time increases, whereas those with shorter correlation length result in a rapid increase in σ_R . Further study might be able to find a definite relationship between the correlation length of random transport property field and the evolution of fluctuation in the flow pattern, to guide the selection of material sample to achieve a required mold-filling result.

The conclusions related to correlation length can be summarized as:

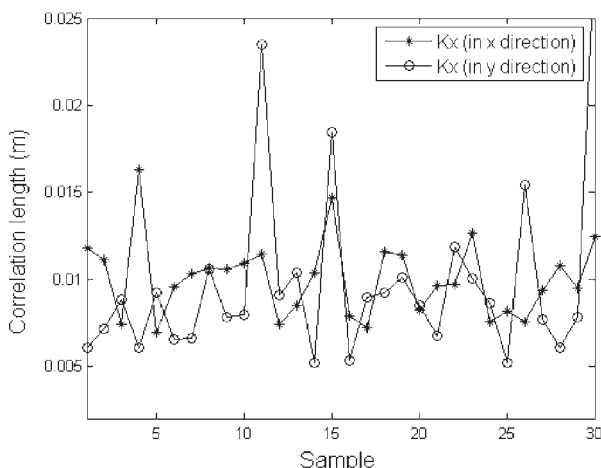
- (1) On average, the correlation length in the x direction is 8.9 mm, 10.1 mm and 11.3 mm for V_f , K_x and K_y , respectively; while that in the y direction is 7.1 mm, 9.8 mm and

8.5 mm for V_f , K_x and K_y , respectively. The correlation length of K_x or K_y is slightly higher than that of V_f , possibly due to the dependence on the clustering morphology of the former.

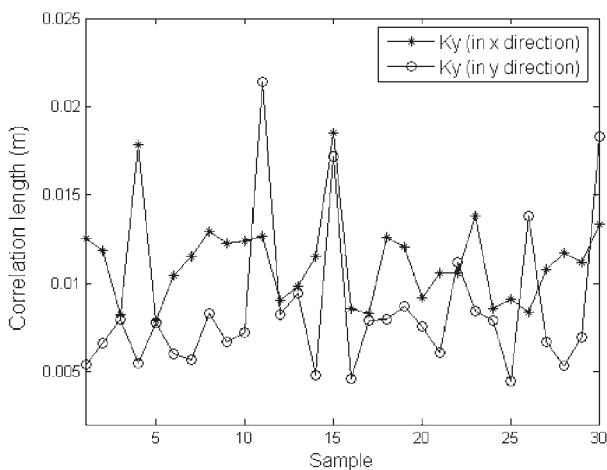
- (2) Though the currently employed sampling region size (about 12 mm) is larger than the fitted correlation length, it can be seen (Fig. 10) that the correlation degree is still significant within a distance of 30 mm for many samples. Therefore, the current sampling size is acceptable.
- (3) The RVE size estimated in Section 4.1 in the x direction is slightly higher than that in the y direction (Fig. 8), which is consistent with the correlation length. There is a proportional relation between the RVE size and the correlation length in different directions, as confirmed by [15].
- (4) For any property, a stronger correlation exists in the x direction, which is the same case as the correlation length defined from the two-point PDF of the 2-phase microstructure (Section 3.2.3). Since all the samples are cut in the same orientation (i.e. the y direction is along the roll production and the x direction the transverse one), the anisotropy in the correlation length might be induced by the fabric generation process.



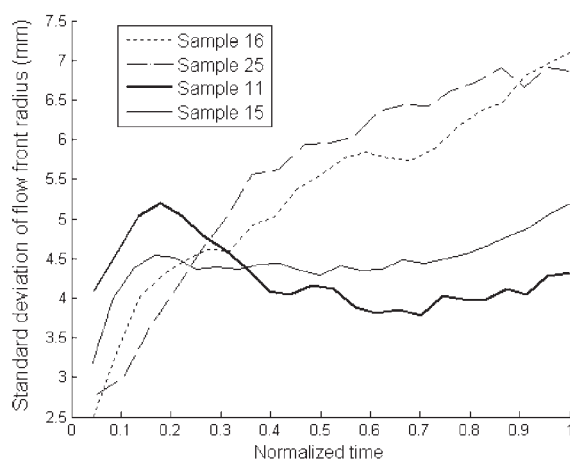
(a) Correlation length of V_f field



(b) Correlation length of K_x field



(c) Correlation length of K_y field



(d) Standard deviation of flow front position evolving with time

Fig. 11. Comparison between different samples.

5. Conclusions

The highly disordered microstructure of the CSM leads to difficulty in the prediction of the permeability field and subsequently of the mold-filling pattern in the LCM processes. A methodology is developed, consisting in processing the gray-scale image of fabric samples to extract the statistical characteristics of the random microstructure, which is then incorporated in the formulation of the effective permeability based on the statistical continuum approach adapted for Darcy's law. The effectiveness of the prediction method for the permeability field for the CSM has been validated by comparing the numerical simulation of mold-filling process with the radial injection experiments. When comparing to the traditional Kozeny–Carman model, the latter is found to be much less accurate in filling pattern prediction, due to the lack of two-point statistics containing clustering and anisotropic information. The effect of the sampling size on the prediction results has been analyzed.

Using the realizations of permeability field evaluated from realistic CSM samples, statistical properties are estimated with the main conclusions:

- (1) To obtain a relative error below 5%, the RVE size for V_f should be larger than $10 \text{ mm} \times 10 \text{ mm}$; whereas for K_x (or K_y), it has to be larger than $475 \text{ mm} \times 375 \text{ mm}$.
- (2) The accurate marginal PDF for V_f , K_x , K_y can be obtained in an exponential form using the MEP. It has been shown that V_f follows a Gaussian distribution, whereas K_x and K_y follow a log-normal PDF.
- (3) The spatial correlation of property fields indicates a slightly dominant correlation in the x direction, possibly due to the anisotropy in the distribution of the fiber strands generated by the non-woven production technology.

The proposed methodology can also be applied to similar heterogeneous fabric, which will be useful for optimizing the fibrous microstructure or the production technology to generate it.

Another technique consists in the moving-window technique combined with the generalized method of cells (GMCs) [16]. It is based on the realistic microstructure (one realization); but the statistical continuum approach gets effective property based on statistical information in the sampling region.

In this paper, the task was just to obtain property field for each sample, so both methods could have been effective. However, with

statistical continuum approach, a smallest sampling region can be taken to be more efficient.

Acknowledgments

The authors wish to thank Assoc. Prof. S. Bickerton and the Center of Advanced Composite Materials (CACM) of University of Auckland (NZ) for the use of the experimental devices to acquire the raw data presented in the article. Also they are grateful to Nord – Pas de Calais Council for funding part of the study.

Appendix A

A.1. Derivation of Eq. (11) [8]

By substituting Eq. (9) into (7), the local flow rate is similarly decomposed into a homogenized part and a fluctuating part:

$$\mathbf{q}(\mathbf{x}) = -\mathbf{k}_m \cdot \nabla p(\mathbf{x}) + \hat{\mathbf{q}}(\mathbf{x}) \quad (\text{A-1})$$

with

$$\hat{\mathbf{q}}(\mathbf{x}) = -\hat{\mathbf{k}}(\mathbf{x}) \cdot \nabla p(\mathbf{x}) \quad (\text{A-2})$$

According to the continuity equation (without internal source):

$$\nabla \cdot \mathbf{q}(\mathbf{x}) = -\mathbf{k}_m \cdot \nabla \cdot \nabla p(\mathbf{x}) + \nabla \cdot \hat{\mathbf{q}}(\mathbf{x}) = 0 \quad (\text{A-3})$$

the governing equation for local pressure is derived as

$$\mathbf{k}_m \nabla^2 p(\mathbf{x}) = \nabla \cdot \hat{\mathbf{q}}(\mathbf{x}) \quad (\text{A-4})$$

By means of the Green function, local pressure solution takes the form

$$p(\mathbf{x}) = p_0 - \int \nabla \mathbf{g}(\mathbf{x}, \mathbf{x}') \hat{\mathbf{q}}(\mathbf{x}') d\mathbf{x}' \quad (\text{A-5})$$

or equivalently (by substituting Eq. (A-2)):

$$p(\mathbf{x}) = p_0 + \int \nabla \mathbf{g}(\mathbf{x}, \mathbf{x}') \hat{\mathbf{k}}(\mathbf{x}') \cdot \nabla p(\mathbf{x}') d\mathbf{x}' \quad (\text{A-6})$$

with Green function

$$\mathbf{g}(\mathbf{x}, \mathbf{x}') = \frac{1}{4\pi \mathbf{k}_m (\mathbf{x} - \mathbf{x}')} \quad (\text{A-7})$$

To get the local pressure gradient, Eq. (A-6) is differentiated as:

$$\nabla p(\mathbf{x}) = \nabla p_0 + \int \mathbf{G}(\mathbf{x}, \mathbf{x}') * \hat{\mathbf{k}}(\mathbf{x}') \nabla p(\mathbf{x}') d\mathbf{x}' \quad (\text{A-8})$$

with the Green operator can be written in deviatoric and spherical parts:

$$\mathbf{G}(\mathbf{x}, \mathbf{x}') = -\frac{1}{2k_m} \mathbf{I} \delta(\mathbf{x} - \mathbf{x}') + \frac{1}{2\pi k_m r^2} (2\hat{\mathbf{n}}\hat{\mathbf{n}} - \mathbf{I}) \quad (\text{A-9})$$

where $\hat{\mathbf{n}} = (\mathbf{x} - \mathbf{x}')/r$ and $r = |\mathbf{x} - \mathbf{x}'|$. Replacing $\nabla p(\mathbf{x}')$ with the first order Taylor term, Eq. (A-8) is approximated by:

$$\nabla p(\mathbf{x}) = \nabla p_0 + \left[\int \mathbf{G}(\mathbf{x}, \mathbf{x}') * \hat{\mathbf{k}}(\mathbf{x}') d\mathbf{x}' \right] \nabla p_0 \quad (\text{A-10})$$

where $\hat{\mathbf{k}}(\mathbf{x}')$ is the random permeability at any $\mathbf{x}' \in V$ for a given $\mathbf{x} \in h$. Taking the expectation of Eq. (A-10), Eq. (11) is obtained.

References

- [1] Arbter R, Beraud J, Binetruy C, Bizet L, Breard J, Comas-Cardona S, et al. Experimental determination of the permeability of textiles: a benchmark exercise. *Composites Part A* 2011;42:1157–68.
- [2] Jaganathan S, Tafreshi HV, Pourdeyhimi B. A realistic approach for modeling permeability of fibrous media: 3-D imaging coupled with CFD simulation. *Mater Sci Eng A* 2008;63:244–52.
- [3] Laschet G, Kashko T, Angel S, et al. Microstructure based model for permeability predictions of open-cell metallic foams via homogenization. *Mater Sci Eng A* 2008;472:214–26.
- [4] Ioannidis MA, Kwiecien MJ, Chatzis I. Statistical analysis of the porous microstructure as a method for estimating reservoir permeability. *J Petrol Sci Eng* 1996;16:251–61.
- [5] Bickerton S, Battley M, Gan JM. Automated characterisation of variability in glass fibre reinforcement architecture. In: 10th International conference on textile composites. Recent advances in textile composites. Lille: Destech Publications; 26–28 October 2010. p. 148–56.
- [6] Garmestani H, Lin S, Adams BL. Statistical continuum theory for inelastic behavior of a two-phase medium. *Int J Plast* 1998;14:719–31.
- [7] Corson PB. Correlation functions for predicting properties of heterogeneous materials. II. Empirical construction of spatial correlation functions for two phase solids. *J Appl Phys* 1974;45:3165–70.
- [8] Li DS, Saheli G, Khaleel M, Garmestani H. Quantitative prediction of effective conductivity in anisotropic heterogeneous media using two-point correlation functions. *Comput Mater Sci* 2006;38:45–50.
- [9] Zhang F, Cosson B, Comas-Cardona S, Binetruy C. Efficient stochastic simulation approach for RTM process with random fibrous permeability. *Compos Sci Technol* 2011;71:1478–85.
- [10] Kroner E. Statistical modelling in modelling small deformation of polycrystals. In: Gittus J, Zarka J, editors. New York: Elsevier Applied Science; 1987. p. 229.
- [11] Adams BL, Canova GR, Molinari A. A statistical formulation of viscoplastic behavior in heterogeneous polycrystals. *Textures Microstruct* 1989;11:57–71.
- [12] Pindera M-J, Khatam H, Drago A, Bansal Y. Micromechanics of spatially uniform heterogeneous media: a critical review and emerging approaches. *Composites Part B* 2009;40:349–78.
- [13] Kanit T, Forest S, Galliet I, Mounoury V, et al. Determination of the size of the representative volume element for random composites: statistical and numerical approach. *Int J Solids Struct* 2003;40:3647–79.
- [14] Pelissou C, Baccou J, Monerie Y, Perales F. Determination of the size of the representative volume element for random quasi-brittle composites. *Int J Solids Struct* 2009;46:2842–55.
- [15] Guilleminot J, Soize C, Kondo D, Binetruy C. Theoretical framework and experimental procedure for modeling mesoscopic volume fraction stochastic fluctuations in fiber reinforced composites. *Int J Solids Struct* 2008;45:5567–83.
- [16] Graham LL, Baxter SC. Simulation of local material properties based on moving window GMC. *Probab Eng Mech* 2001;16:295–305.